

Article

Surface Deposition on Titania in a Physiological Solution with Ultraviolet Irradiation In Situ and Effect of Heat Treatment

Chun-Yang Su, Qing Zhou *  and Cheng-Hong Zou 

College of Mechanical and Electric Engineering, Nanjing University of Aeronautics and Astronautics, Nanjing 210016, China; xiaosucy@gmail.com (C.-Y.S.), alexzou29@gmail.com (C.-H.Z.)

* Correspondence: anzhouqing@nuaa.edu.cn

Received: 27 November 2018; Accepted: 26 January 2019; Published: 29 January 2019



Abstract: Photocatalysis-enhanced surface deposition on titanium surfaces for biomedical applications is investigated in this work. Immersion tests of commercially pure titanium (CP-Ti) pieces in a simulated body fluid adding bovine serum albumin (BSA) under ultraviolet (UV) irradiation in situ are carried out. The morphologies of deposition are characterized by SEM and stereo imaging microscopy, and the quantity and composition of the deposition is examined by SEM, energy dispersive spectroscopy (EDS) and X-ray photoelectron spectroscopy. The results show a deposition layer with thickness 89 μm is produced on 600 °C heat-treated specimens. An irradiation pattern of lighting/dark repeated results in more deposition on heat-treated CP-Ti. It is confirmed that a mixture of anatase and rutile phases generated on 600 °C heat-treated specimens has enhanced photocatalysis. The decomposition of BSA by photocatalysis, a possible product of nitrite also results in enhanced deposition on Ti. EDS analysis shows large reduction of carbon in the deposition on UV-light exposed surfaces compared to no UV-light-exposed surfaces. Furthermore, C–H bond decreases and C–C, Ca–O, and P–O bond increases are found on photoactivated surfaces. The deposition produced by this method is expected to be useful for applications to biomaterials with high bioactivity.

Keywords: surface deposition; photocatalysis; bovine serum albumin; simulated body fluid; anatase; rutile; CP-Ti

1. Introduction

Physicochemical exchange between metal surfaces and physiological surrounds has been subjected to extensive studies [1–8] because this behavior is closely related to the biological performance of metals. The surface of titanium metal when immersed in a physiological solution is subjected to repassivation processes. This repassivation behavior is accompanied by the precipitation of compounds from solution [1–4]. Surface adsorption and deposition understanding due to different electrochemical properties between metal surfaces/solutions [5–7] is important for the purpose of generating strong bonding between the implant/tissue interface, and is helpful for elucidating the mechanism of biomineralization. It has been pointed out that ultraviolet (UV) light irradiation enhances surface hydrophilicity and decreases hydrocarbon content of the deposition and improves bioactivity [8–17]. UVA (wavelength 365 nm) and UVC (wavelength 250 nm) are both capable of producing a superhydrophilic surface. Only UVC which has higher energy is effective in removing hydrocarbons from the surface deposition [9]. Basically titania, or TiO_2 , is known as an excellent photocatalyst. A hole-electron pair is produced in titania by a photon activation when the photon is absorbed by the titania and has energy larger than or equal to the band gap of the titania. The hole and electron take part in oxidative and reductive reactions with water molecules, respectively,

which produce highly active hydroxyl radical products. Because the surface of titanium generally absorbs water and organic impurities from the atmosphere [9], it is possible that water splitting on the surface occurs first due to photocatalysis. It is supposed the behavior of the hydroxyl radicals produced by water splitting plays important role in causing superhydrophilicity and removal of hydrocarbons.

UV light irradiation has also been applied to assisting apatite formation on titanium [18–22]. Shozui [18] used heat-treated titanium pieces treated with UV light irradiation as the object. He found UV irradiation enhances apatite formation on titanium after an immersion of the titanium in Kokubo's simulated body fluid (SBF). A titanium surface treated by H₂O₂ oxidation and subsequent calcination was subjected to UV irradiation in air and in water [19,20]. It was reported that more active sites of TiOH groups produced on titanium surfaces in water are responsible for more nucleation of apatite. Bone-like apatite precipitation has been reported as being produced on anodized titanium when the anodized titanium was immersed in SBF under UVC light irradiation [21,22]. The conclusion showed that hydroxyl radicals induced by photocatalysis provide more nucleation sites for apatite precipitation.

In this work, the effects of UV light irradiation on the generation of surface depositions on titanium metals when the titanium is immersed in an SBF to which bovine serum albumin has been added is investigated. An exposure pattern of lighting/dark repeated is used in UV lighting for the purpose of generating more deposition. In addition, different heat-treatment methods are applied to prepare for the titanium specimens with different surface phases. It is known that two main polymorphs exist in titania, these being anatase and rutile. These two phases have different photocatalysis [23–25]. Chemical formation on immersed surface is checked by diverse methods, such as scanning electron microscopy, energy-dispersive X-ray spectrometry and X-ray photoelectron spectroscopy.

2. Materials and Methods

Commercially pure titanium (CP-Ti, Grade 2) bars with 16 mm diameter (Baoji Titanium Industry Ltd., Baoji, China) were obtained and wire-cut into 2 mm thickness pieces. Three types of pieces for immersion tests were prepared: polished, and heat-treated at 400 and 600 °C. The polished specimens were prepared through grinding by using abrasive papers until 1000# and then polishing with W1.5 and 0.5 alumina powder. Heat treatments were carried out by heating the polished pieces to 400 and 600 °C, holding them for 1.5 h in an argon-gas protected electric furnace and then quenching them in water. These specimens were then ultrasonically cleaned in distilled water and held in a vacuum drying oven. Before immersion testing, the three types of surfaces were examined by X-ray diffraction (XRD, Ultima IV, Rigaku, Tokyo, Japan) to determine crystal forms. The surface roughness was probed by a 3D-imaging microscope (VHX-1000, Keyence, Osaka, Japan)

Immersion testing of CP-Ti pieces was carried out under UV light irradiation as schematically shown in Figure 1. A Tris-HCl buffered SBF containing 27 mM HCO₃⁻ was used. The composition of the SBF is 142 Na⁺, 125 Cl⁻, 27 HCO₃⁻, 5 K⁺, 1.5 Mg²⁺, 2.5 Ca²⁺, 1 HPO₄²⁻, and 0.5 SO₄²⁻ (mM/L). 0.8 g/L bovine serum albumin (BSA) was added to the SBF to simulate human plasma. An 18 W Hg UVC lamp (KADIND, Shaoxin, China) with a 303 mm length was used as light source. The UVC lamp was hung 150 mm above table. An irradiation pattern of 4 h UVC lighting and 20 h dark was set for one daily period. Att [9] has reported that an aged titanium in dark condition has inferior bioactivity to UV light activated titanium. However, the reactivation of the aged titanium promotes more bioactivity. We utilized this lighting/dark pattern to attempt to produce more deposition on CP-Ti. The surfaces of CP-Ti pieces were irradiated repeatedly for 15 days. A dark environment was realized by covering the glass dishes and covering the water-bath with a black cover.

The pieces after immersion were cleaned with distilled water and dried with a dryer. After this, the surface morphologies of the immersed pieces were observed by using a scanning electronic microscope (SEM, JSM-6360LV, JEOL, Tokyo, Japan). The surface composition was examined by using an energy-dispersive X-ray spectrometer (EDS, GENESIS 2000 XMS 60) attached to the SEM. X-ray photoelectron spectroscopy (XPS, PHI Quantera II, Chanhassen, MN, USA) was also used for surface composition and chemical bond determination. During XPS testing, a monochromatic AlK

X-ray source with a pass energy of 280 and 55 eV for survey scan and high-resolution scan was used, respectively. A take-off angle of 45° to the surface normal was used for each specimen. An area of $100 \mu\text{m} \times 100 \mu\text{m}$ was detected either for survey or for high resolution scan.

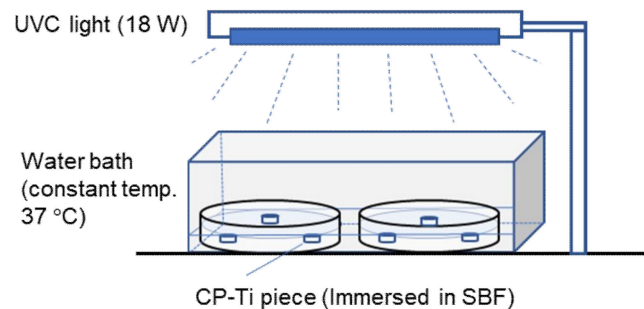


Figure 1. Schematic drawing of apparatus for immersion tests of CP-Ti with UV light irradiation.

3. Results

3.1. Surface Characterization before Immersion

Figure 2 shows XRD results of polished, and 400 and 600 °C heat-treated (HT) CP-Ti. X-ray powder diffraction spectra of anatase and rutile was utilized to identify the phases presented in the XRD results of the CP-Ti surfaces. In Figure 2 it can be seen besides titanium peaks, anatase and rutile peaks are present for the 600 °C HT surface. Anatase peaks can be identified for the 400 °C HT surface. Figure 3 shows specimen appearances before and after immersion. Multiple colors are illustrated on different specimens before immersion. A brown color is shown on the surface of the 400 °C HT specimen, whereas a pale blue color is shown on the surface of the 600 °C HT specimen. Considering the phase of anatase generated on the 400 °C HT specimen and the mixture phase of anatase and rutile generated on the 600 °C HT specimen, it is possible that the brown is the color of anatase, and the pale blue is the color of rutile [26].

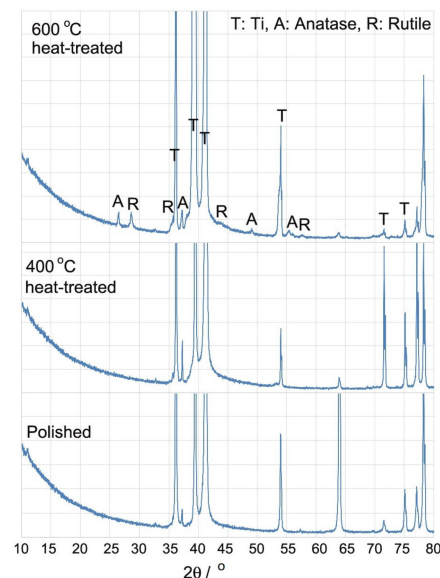


Figure 2. X-ray diffraction spectra of CP-Ti specimens after mechanical polishing, and 400 and 600 °C heat treatment, before immersion.

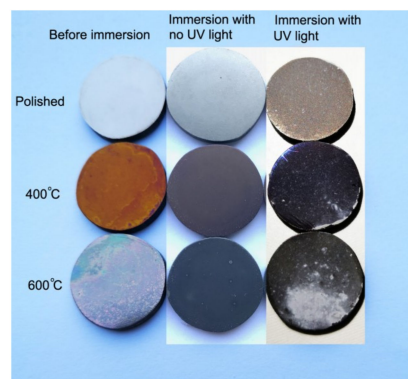


Figure 3. Comparison of CP-Ti pieces' appearances before and after immersion. The pieces' appearances with no UV light irradiation is also shown.

SEM morphologies and 3D imagings of the CP-Ti pieces before immersion are shown in Figure 4. It is shown in SEM micrographs that the surface morphologies on the polished and the 400 °C HT specimens (Figure 4a,b) are similar. However, a feature of crystallization can be observed on the 600 °C HT surface (Figure 4c) which corresponds to crystals of anatase and rutile being generated at this temperature. The stereo imagings used here to characterize the surface roughness at the microscale is shown in Figure 4d–f. By measuring the contour of the line segment on the stereo micrographs it is shown that the roughness of the three types of surfaces is almost the same. The maximum heights of the contour R_z are near 35 μm for three types of specimens. To understand the effect of nanosized contours on adsorption, roughness at the ranges of sub-microscale or nanoscale should be further investigated.

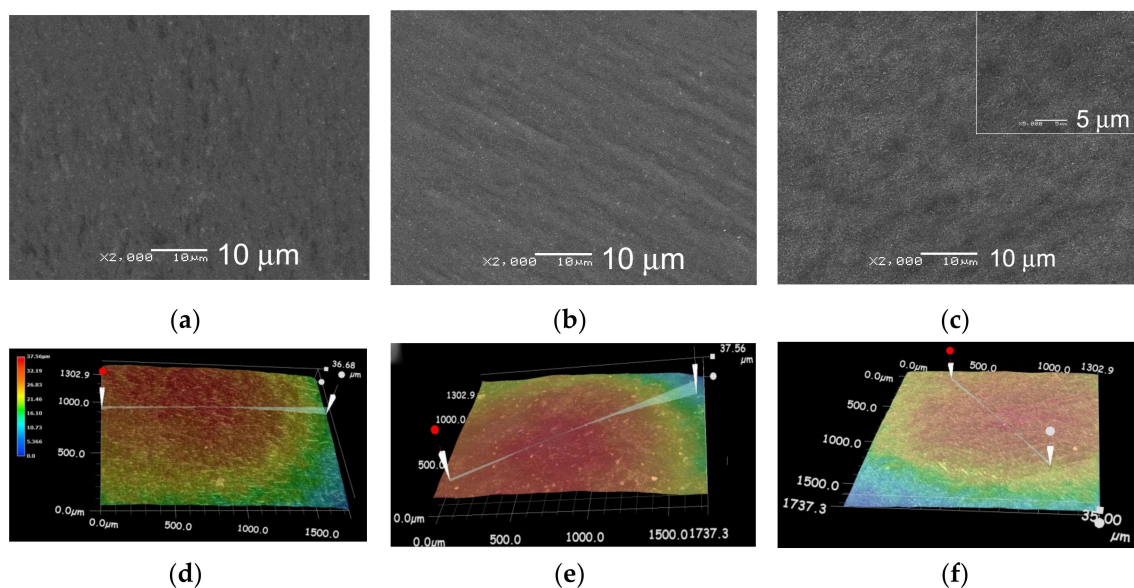


Figure 4. Surface characterization of CP-Ti by SEM of (a) polished, and (b) 400 °C, and (c) 600 °C heat-treated specimens and stereo imaging showing surface contours of (d) polished, and (e) 400 °C and (f) 600 °C heat-treated specimens.

3.2. Deposition Characterization and Composition

The morphologies of the surfaces after bare immersion (immersion without UV light irradiation) and the surfaces after immersion with UV light irradiation are shown in Figure 5. A cloud-like substance which may be the deposition of BSA is observed on bare-immersed surfaces. The N element presence in Table 1 explains BSA adsorption on Ti. Previous studies by Burgos-Asperilla [3] showed the adsorption of BSA on titanium occurs in advance of CaP deposition. Square-shaped salt crystals

deposited on the surfaces of bare immersion are confirmed. A hole with a size of near 5 μm (Figure 5a) is believed to be a remain left behind of a salt particle. A comparison of three photographs (Figure 5a–c) shows almost no difference in deposition quantity on the three types of specimens indicating the adsorption capacity due to heat treatment effect is almost the same on the surfaces without UV irradiation. The amount of deposition on the specimens without UV irradiation is much less relative to those produced on the specimens with UV irradiation (Figure 5d–f). The surfaces with UV light irradiation (Figure 5d–f) show small particle and powder-like features. A thicker deposition layer is generated (Figure 3) particularly on 600 °C HT pieces under UV irradiation. Less deposition is seen on 400 °C HT surfaces than on 600 °C HT surfaces. The deposition is the least on the polished surface. The results imply that the effects of heat treatment on surface deposition are significant under UV light irradiation.

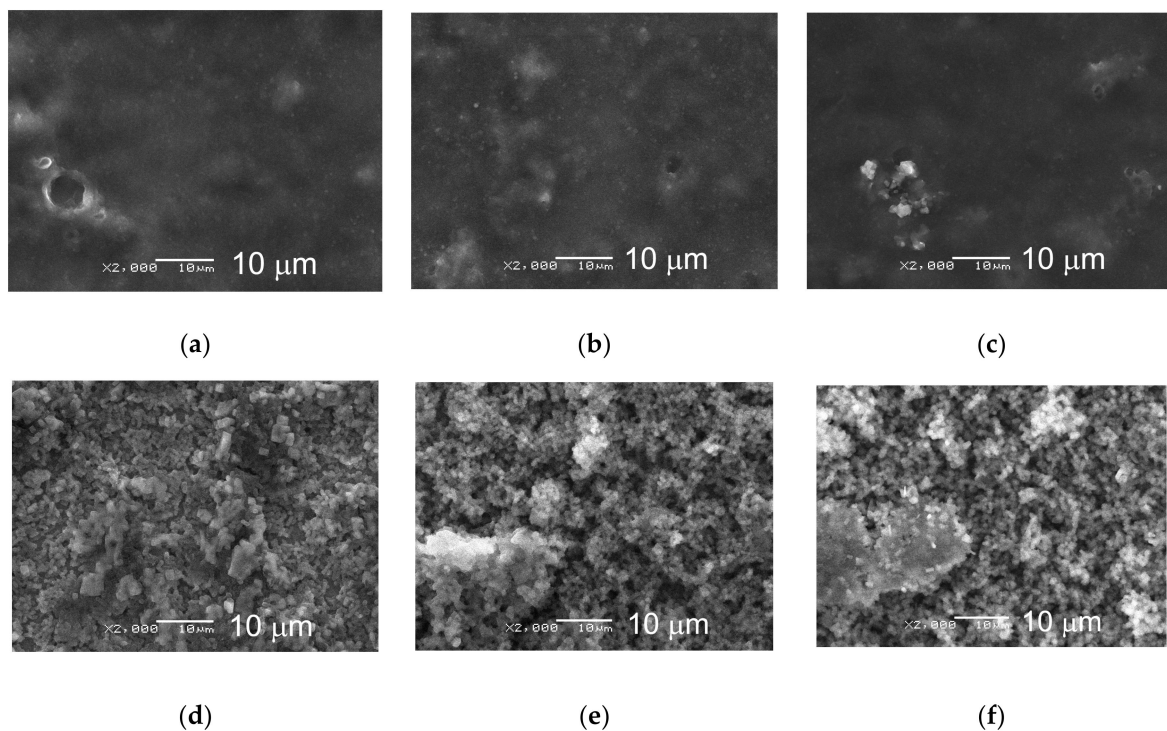


Figure 5. SEM surface morphologies of (a) polished, (b) 400 °C, (c) 600 °C heat-treated CP-Ti specimens after immersion with no UV light irradiation, (d) polished, (e) 400 °C, (f) 600 °C heat-treated specimens after immersion with UV light irradiation.

A method of stereo imagination was used for the measurement of deposition thickness, with the results shown in Figure 6. The layers were partially separated from the substrate when measuring so as to the thickness could be measured. The height difference between the layers and substrate was obtained and regarded as the thickness. The thickness in thick areas is 19–21 μm and 62–89 μm for the 400 °C and 600 °C HT CP-Ti pieces, respectively. Due to nonuniformity the thicknesses of the depositions in other areas are thinner. As shown in Figures 3 and 5 the distribution of the depositions is uneven. A larger area of white deposition can be observed on the surface of the 600 °C HT pieces. Besides this there are also some islands of deposition (Figure 3). On the surface of the 400 °C HT pieces, the deposition is relatively uniform, however, concentration of the deposition on many islands and the edges can be observed. Only a small number of islands can be seen on the polished surfaces.

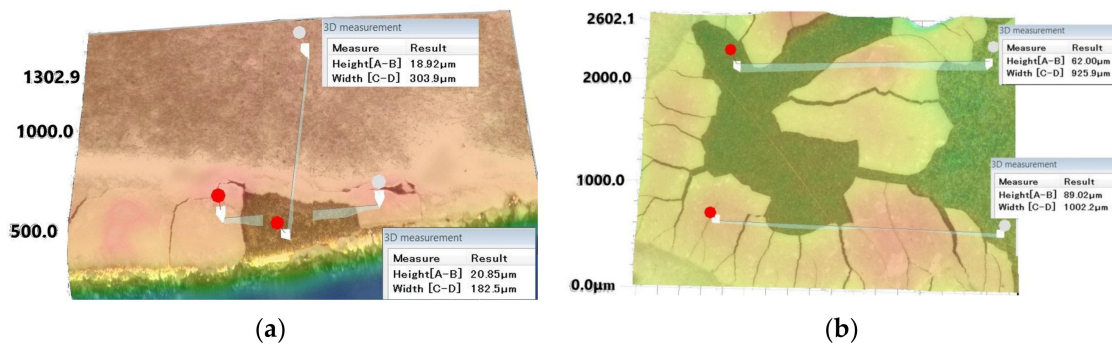


Figure 6. Deposition thickness measurement by stereo imaging on (a) 400 °C heat-treated CP-Ti and (b) 600 °C heat-treated CP-Ti after immersion with UV irradiation.

Figure 7a shows further a SEM micrograph of the deposition on the thin thickness areas treated with UV light irradiation. Two kinds of particles—rod-shaped and cube-shaped—were found. The EDS detection of the rod-shaped particles (Figure 7b) denotes that it contains mainly C, O, Ti, Na, Cl, Ca and P elements. Because the electron beam size used in EDS examination (2 μm) exceeds the size of the rod-shaped particles, the elements should include those both in the rod-shaped and in the cube-shaped particles. It will be demonstrated later that the cube-shaped particles are the crystals of salt. Consequently the rod-shaped particles are composed of C, O, Ti, Ca and P. The N element included in BSA was removed from the deposition due to the photocatalysis-causing deamination. The Ca and P elements were precipitated from SBF solution. Histograms of the length and width of particles are shown in Figure 7c,d respectively. According to the histograms the length and width of the rod-shaped particles are estimated to be around 1.4 and 0.67 μm, respectively. The cube-shaped NaCl crystals are 1–4 μm in size. Large NaCl crystals of around 50 μm were also found.

The stability of the deposition layer generated was checked by a test of ultrasonic vibration. A 40 kHz frequency ultrasonic treatment lasting 5 min was used to attempt to damage the deposition when the pieces were soaked in distilled water. The results are shown in Figure 8. It can be seen that except for a little layer separation the rest of the deposition remained complete on the 600 °C HT surface. The deposition on the 400 °C HT pieces remained totally complete. These results explain the higher stability of the deposition produced on heat-treated CP-Ti under UV light irradiation.

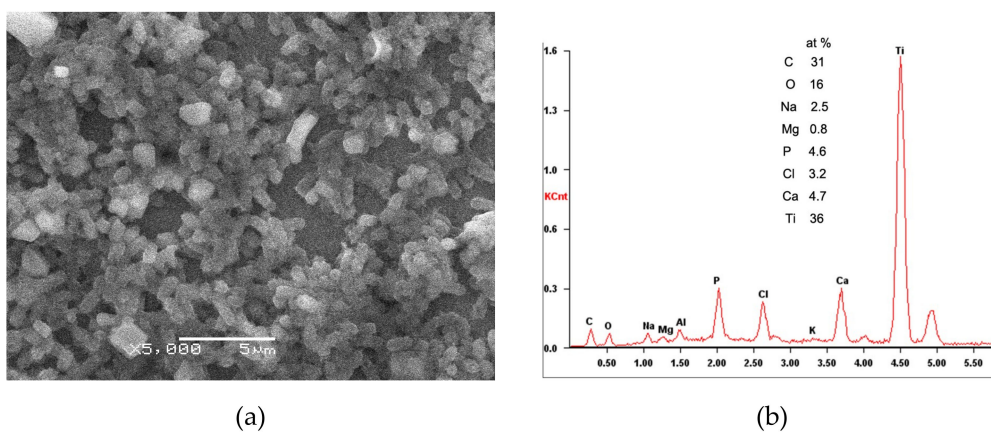


Figure 7. Cont.

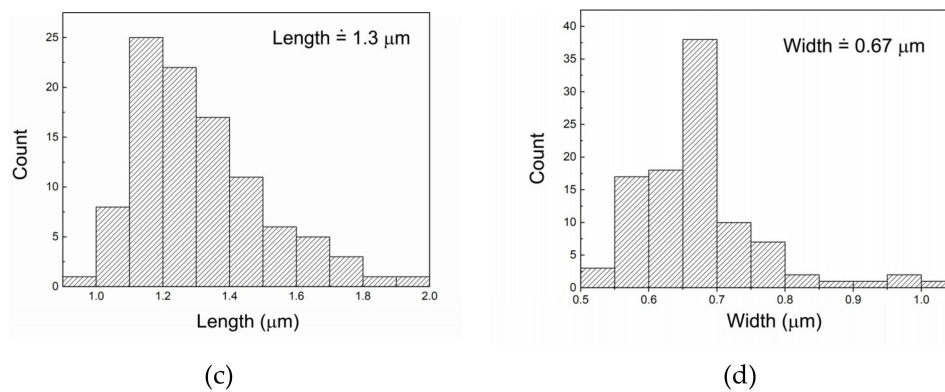


Figure 7. SEM micrograph of the deposition produced by immersion with UV light irradiation (a) heat treated surface at 400 °C, (b) EDS analysis of the rod particle and (c) histograms of length distribution and (d) wider distribution of rod-shaped particles. Length and width are measured on 100 randomly selected rod-shaped particles.

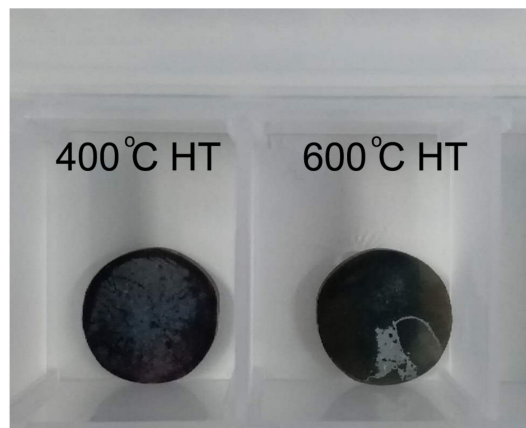


Figure 8. Pieces after ultrasonic vibration testing used to check the stability of deposition.

The compositions of the depositions measured by EDS are listed in Table 1. It may be noted that the elements of C, O, Ti, Na, Mg, Cl, K, Ca, and P are present on all surfaces. Aluminum element is present on the surface of the pieces which underwent UV light irradiation, while not present on the surfaces which did not undergo UV light irradiation, and is considered to be induced by the polishing agent. Nitrogen is found on the pieces which did not undergo UV light irradiation, but is not found on the pieces which did undergo UV light irradiation. BSA contains amino acids which include N elements. This indicates that the UV irradiation has influences on the decomposition of amino acids and causes deamination.

It was found that the amount of carbon deposited on UV-light-irradiated specimens was much less than those on no-UV-light-irradiated specimens (Table 1). Inversely, the elements of O, Ti, Na, Mg, Ca, and P are shown to have larger contents on UV-light irradiated pieces compared to no-UV-light irradiated pieces. The amount of increment differs between the elements, with larger increments of O, Ti, Ca and P, and smaller increments of Na and Mg.

It was also found that there were different amounts of deposition on surfaces subjected to different heat treatment methods under UV light irradiation. More C, Mg, Cl, Ca and P elements were deposited on HT pieces compared to polished ones. Amounts increased with the heating temperature. However, the Ti atomic percentage on HT pieces is largely decreased compared to the polished pieces, indicating the difficulty of Ti diffusion as the deposition thickens. However, all the elements deposited on CP-Ti without UV light irradiation showed no large differences between the HT and polished surfaces.

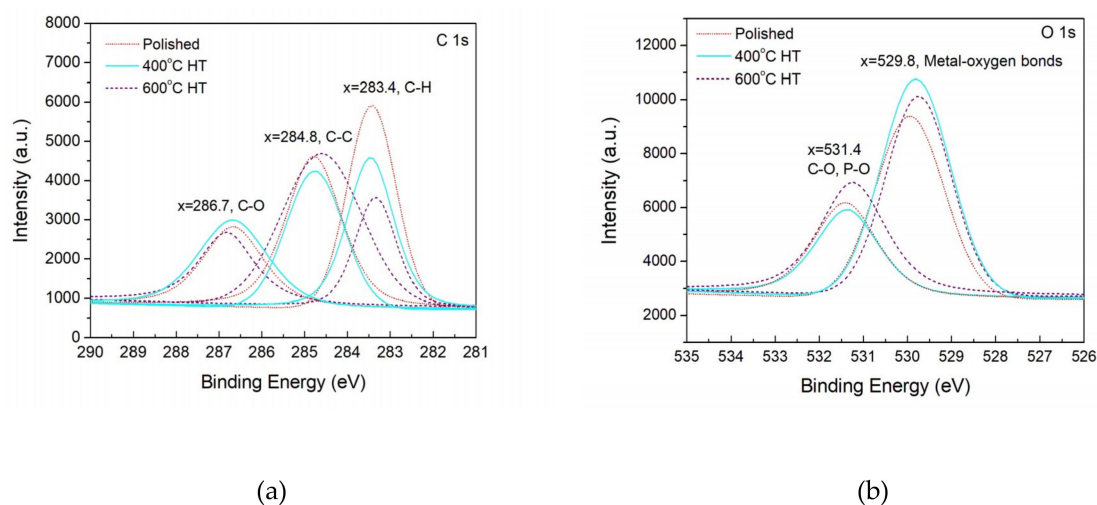
Table 1. Composition of the surfaces after immersion in simulated body fluid (+0.8 g/L bovine serum album) detected by Energy-dispersive X-ray spectrometer (at %).

Surface Types		C	O	Ti	N	Na	Mg	Al	Cl	P	Ca
UV light immersion	Polished	29.8	15.2	42.1	-	3.3	0.3	0.7	2.7	2.8	2.6
	400 °C HT	38.7	14.4	28.2	-	5.4	0.3	0.7	4.6	3.5	3.8
	600 °C HT	46.7	13.6	13.9	-	4.7	0.4	0.5	6.1	6.0	7.7
No UV light immersion	Polished	69	9.2	11.5	2.0	2.1	0.2	-	3.8	0.9	0.8
	400 °C HT	70.2	9.7	9	2.3	2.2	0.3	-	4.1	1.1	0.9
	600 °C HT	68	9.7	12.7	1.6	2.1	0.2	-	3.2	1.1	1.0

3.3. XPS of Deposition

Figure 9 shows high resolution XPS of C1s, O1s, Ca2p and P2p for the specimens with UV light irradiation. These spectra have been corrected by assuming a standard C–C peak at 284.8 eV. The spectra of C1s are deconvoluted into three sub-peaks as shown in Figure 9a. According to the bonding energy of C1s [27], C–H, C–C and C–O correspond to three peaks at 286.7, 284.8, and 283.4, respectively. Furthermore, it can be observed semi-quantitatively that the intensity of C–H bonds deposited on the 400 and 600 °C HT surfaces is much lower than that deposited on the polished surfaces. By contrast, the intensity of C–C peaks shown on the HT surfaces is higher than that for the polished surfaces. Particularly, a wider C–C peak for 600 °C HT surfaces can be seen indicating larger production of C–C by 600 °C HT. Near the same intensity of C–O peaks for the three types of surfaces was identified.

The O1s spectra (Figure 9b) can be deconvoluted into two sub-peaks: metal-oxygen bonds at 529.8 eV and C–O and P–O bonds at 531.4 eV. Figure 9b shows that the intensity of the metal-oxygen bond on the 400 °C HT surfaces is the largest among the three types of specimens, whereas the largest intensity of organic forms of oxygen bonds occurs for the 600 °C HT surfaces. The Ca2p spectra (Figure 9c) show spin-orbit splitting at 2p_{1/2} and 2p_{3/2} at the bonding energies of 345.8 and 349.3 eV, respectively. They both indicate the formation of a Ca–O bond. Also by observed from the peak intensity it is semi-quantitatively described that the larger Ca–O bond is produced on the HT pieces. The P2p spectra (Figure 9d) are deconvoluted into two sub-peaks at 131.4 and 132.3 eV. With regard to the XPS NIST (National Institute of Standards and Technology) [27] database, these two peaks correspond to PO(C₆H₅)₃ and P(C₆H₅)₃ bonds, respectively. There is larger deposition of PO(C₆H₅)₃ and P(C₆H₅)₃ bonds on the HT pieces than on the polished surfaces. Large increment of PO(C₆H₅)₃ bonds on the 600 °C HT surface is noticed compared to other two types of surfaces.

**Figure 9.** Cont.

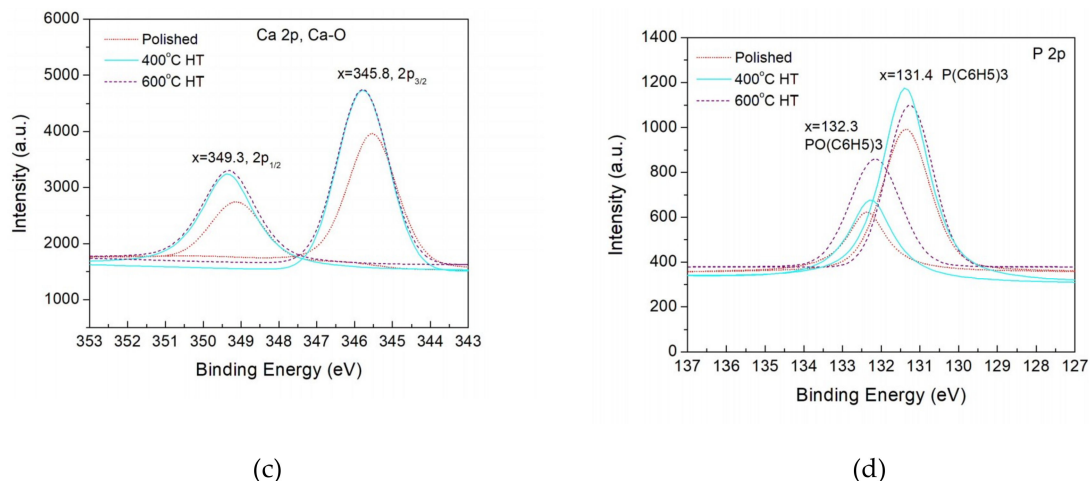


Figure 9. High resolution XPS analysis of the deposition on the surfaces after UV light irradiated immersion. (a) C1s, (b) O1s, (c) Ca2p and (d) P2p.

4. Discussion

The above results demonstrate that UV light irradiation is effective in promoting more deposition on heat-treated titanium surfaces. The bonding of the deposition to the surface of titania is relatively strong and can withstand ultrasonic vibration. Lee [21,22] has previously investigated bone-like apatite formations on anodized surfaces of titanium in an SBF with UV irradiation. His immersion tests were performed under constant UV irradiation (7 days) with no BSA addition into the SBF. The thickness of the bone-like apatite formed was much less than that obtained in this work. The amount of deposition is affected by many factors. Surface structure, different photocatalysis between anatase and rutile, and the experimental conditions are three factors which will be discussed in the follows.

Surface structure expressed by the parameter of surface roughness is a factor that influences initial adsorption to surfaces. In this work, near the same microscale roughness for three types of pieces was obtained after heat treatments. The effect of the roughness at the nanoscale is unknown. If heat-treatment-caused phase transformation generated surface roughness at the nanoscale, there should have been an effect of heat treatment on the deposition. The results actually obtained from the bare immersion tests indicate that there is no effect of heat treatment on the deposition without UV irradiation. The obstacle of BSA which adsorbed on the surface of the titania first from further deposition can be considered as the reason [3].

Different photocatalysis between anatase and rutile has been reported [23]. Anatase is unstable i.e., in a higher energy state providing more localized states and resulting in more adsorbed hydroxyl radicals under the action of photons, which gives rise to higher photocatalysis of anatase than rutile. However, rutile is considered to have higher free surface energy than anatase, leading to more adsorption of active ions and molecules. There is also an adverse debate about the photocatalysis difference between rutile and anatase [23]. Increased photocatalysis on a mixed-phase (anatase and rutile) titania has been demonstrated in many works [23]. The theoretical interpretation of this attributes the phenomenon to electron transfer between rutile and anatase, resulting in an improvement to oxidative reaction.

The experiments related to the surface adsorption behavior in this work have two aspects, the UV exposure pattern and the BSA solution. Att [9] attributes different bioactivity between aged titanium surfaces and aged-UV-treated surfaces to the amount of carbon deposited on surfaces. In dark immersion the surface carbon is deposited more than that under UV light. Greater amounts of hydrocarbon deposition impair bioactivity. A dark aged surface reactivated by UVC irradiation leads to enhanced hydrocarbon decreases in deposition. The UV irradiation pattern of lighting/dark used in this work can largely remove hydrocarbon from the deposition. Reduced hydrocarbon consequently gives rise to higher bioactivity and more deposition is predictable.

Furthermore, the adsorption and photodegradation of BSA is closely related to the enhanced deposition on the Ti. It has been reported [3] that the absorption of BSA to the surface of titanium occurs before CaP deposition. This implies that BSA decomposition is subsequent to BSA adsorption. The degradation of BSA under UV irradiation is a process of macromolecular chain breaking [28] and release of CO₂ [29]. Yamamoto [30] has reported the cell adsorption capacity of an organosilane monolayer covered by serum albumin after UV light degradation is increased. Release of nitrite was demonstrated in the procedure of protein nitration under solar radiation by Meusel [31] when BSA and ovalbumin were used as model proteins. Nitrite presence further facilitates the oxidation of proteins and accelerates the photodegradation of BSA [32,33]. These investigations are helpful to understanding enhanced deposition on photoactivated surfaces in the presence of BSA. The debonding of the ammonia component results in a C–C framework remaining [34,35] which may give rise to the enhanced C–C bond amounts on photoactivated surfaces (600 °C HT surfaces). The increments in P–O and Ca–O bonds in the deposition are also correlated to the photodegradation of amino acids involving the precipitation behavior of calcium and phosphate ions. Further investigation in this point is needed.

Thus, the deposition layers produced by immersion in BSA added SBF under UV light irradiation give reduced amounts of C–H bonds and large amounts of Ca–O and P–O bonds. This kind of layer possesses more potential to facilitate the improvement of bioactivity, which may see its application in the field of high bioactive biomaterials.

5. Conclusions

An investigation on UVC irradiation in situ for surface modification and surface deposition on CP-Ti has been performed in this work. A simulated body solution adding bovine serum albumin was used in the immersion tests under UVC irradiation. The light irradiation was patterned with 4 h lighting and 20 h dark for one daily period and lasted 15 days. A thicker deposition layer was produced on heat-treated CP-Ti compared to the bone-like apatite layer previously obtained by others. The precipitation of hydrocarbon on UV-irradiated surface was much less than that on no-UV-irradiated surfaces. The lighting/dark pattern of UVC radiation is considered to be the reason for large reductions of C–H bonds and for the causing of more deposition on the photoactivated surfaces. By XPS it was found that C–C, Ca–O, and P–O bonds in the deposition were all increased on the photoactivated surfaces. These phenomena were correlated to the decomposition of amino acids by photocatalysis including the precipitation of calcium and phosphate ions from SBF. The enhanced photocatalysis in the nitration of BSA when the BSA is adsorbed on the titania is also a possible contribution to the enhanced deposition on heat-treated pieces.

On anatase surfaces (heat-treated at 400 °C) a layer of thickness 21 µm and on the surface of the mixture of anatase and rutile (heat-treated at 600 °C) a layer of thickness 89 µm was generated. The distribution of the deposition was not uniform, and was concentrated in islands and on edges. The deposition was mainly composed of rod-shaped particles with 1.3 µm length and 0.7 µm width. The stability of the layer was high enough to withstand ultrasonic vibration. Because the deposition has such advanced properties as described in the above, the application of the deposition layer for biomaterials with high bioactivity is expected.

Author Contributions: Conceptualization, C.-Y.S. and Q.Z.; Methodology, C.-H.Z.; Software, C.-Y.S.; Validation, Q.Z.; Formal Analysis, C.-H.Z.; Investigation, Q.Z.; Resources, Q.Z.; Data Curation, C.-H.Z.; Writing—Original Draft Preparation, Q.Z.; Writing—Review and Editing, Q.Z.; Visualization, C.-Y.S.; Supervision, Q.Z.; Project Administration, Q.Z.

Funding: This research received no external funding.

Acknowledgments: We are grateful for the support of XPS figures drawn by Zheng, J.J., a graduate student from Nanjing University of Aeronautics and Astronautics.

Conflicts of Interest: The authors declare no conflict of interest.

References

1. Alkhateeb, E.; Virtanen, S. Influence of surface self-modification in Ringer's solution on the passive behavior of titanium. *J. Biomed. Mater. Res. Part A* **2005**, *75*, 934–940. [[CrossRef](#)] [[PubMed](#)]
2. Asri, R.I.M.; Harun, W.S.W.; Samykano, M.; Lah, N.A.C.; Ghani, S.A.C.; Tarlochan, F.; Raza, M.R. Corrosion and surface modification on biocompatible metals: A review. *Mater. Sci. Eng. C* **2017**, *77*, 1261–1274. [[CrossRef](#)]
3. Burgos-Asperilla, L.; Garcia-Alonso, M.C.; Escudero, M.L. Study of the interaction of inorganic and organic compounds of cell culture medium with a Ti surface. *Acta Biomater.* **2010**, *2*, 652–661. [[CrossRef](#)]
4. Metikos-Hukovic, M.; Katic, J.; Grubac, Z.; Roncevic, I.S. Electrochemistry of CoCrMo implant in Hanks' solution and mott-schottky probe of alloy's passive films. *Corrosion* **2017**, *73*, 1401–1412. [[CrossRef](#)]
5. Walivaara, B.; Aronsson, B.; Rodahl, M.; Lausmaa, J.; Tengvall, P. Titanium with different oxides-in vitro studies of protein adsorption and contact activation. *Biomaterials* **1994**, *15*, 827–834. [[CrossRef](#)]
6. Traini, T.; Murmura, G.; Sinjari, B.; Perfetti, G.; Scarano, A.; D'Arcangelo, C.; Caputi, S. The surface anodization of titanium dental implants improves blood clot formation followed by osseointegration. *Coatings* **2018**, *8*, 7. [[CrossRef](#)]
7. Arvidsson, S.; Askendal, A.; Tengvall, P. Blood plasma contact activation on silicon, titanium and aluminium. *Biomaterials* **2007**, *28*, 1346–1354. [[CrossRef](#)]
8. Ueno, T.; Ikeda, T.; Tsukimura, N.; Ishijima, M.; Minamikawa, H.; Sugita, Y.; Yamada, M.; Wakabayashi, N.; Ogawa, T. Novel antioxidant capability of titanium induced by UV light treatment. *Biomaterials* **2016**, *108*, 177–186. [[CrossRef](#)]
9. Att, W.; Hori, N.; Iwasa, F.; Yamada, M.; Ueno, T.; Ogawa, T. The effect of UV photofunctionalization on the time-related bioactivity of titanium and chromium-cobalt alloys. *Biomaterials* **2009**, *30*, 4268–4276. [[CrossRef](#)] [[PubMed](#)]
10. Tsukimura, N.; Yamada, M.; Iwasa, F.; Minamikawa, H.; Att, M.; Ueno, T.; Saruwatari, L.; Aita, H.; Chiou, W.-A.; Ogawa, T. Synergistic effects of UV photofunctionalization and micro-nano hybrid topography on the biological properties of titanium. *Biomaterials* **2011**, *32*, 4358–4368. [[CrossRef](#)] [[PubMed](#)]
11. Yang, Y.; Zhou, J.; Liu, X.; Zheng, M.; Yang, J.; Tan, J. Ultraviolet light-treated zirconia with different roughness affects function of human gingival fibroblasts in vitro: The potential surface modification developed from implant to abutment. *J. Biomed. Mater. Res. Part B* **2015**, *103*, 116–124. [[CrossRef](#)] [[PubMed](#)]
12. Li, S.; Ni, J.; Liu, X.; Zhang, X.; Yin, S.; Rong, M.; Guo, Z.; Zhou, L. Surface characteristics and biocompatibility of sandblasted and acid-etched titanium surface modified by ultraviolet irradiation: An in vitro study. *J. Biomed. Mater. Res. Part B Appl. Biomater.* **2012**, *100*, 1587–1598. [[CrossRef](#)] [[PubMed](#)]
13. Han, Y.; Chen, D.; Sun, J.; Zhang, Y.; Xu, K. UV-enhanced bioactivity and cell response of micro-arc oxidized titania coatings. *Acta Biomater.* **2008**, *4*, 1518–1529. [[CrossRef](#)] [[PubMed](#)]
14. Narkevica, I.; Reinis, A.; Bugovecka, L.; Skadins, I.; Sansonetti, E.; Kroica, J.; Ozolins, J. In vitro bioactivity and bacteriostasis effect of thermally treated and UV-light irradiated TiO₂ ceramics. *Key Eng. Mater.* **2016**, *674*, 121–126. [[CrossRef](#)]
15. Omid-Bakhtiari, M.; Nasr-Esfahani, M.; Nourmohamadi, A. TiO₂-bioactive glass nanostructure composite films produced by a sol-gel method: In vitro behavior and UV-Enhanced bioactivity. *J. Mater. Eng. Perform.* **2014**, *23*, 285–293. [[CrossRef](#)]
16. Unossona, E.; Welch, K.; Perssona, C.; Engqvista, H. Stability and prospect of UV/H₂O₂ activated titania films for biomedical use. *Appl. Surf. Sci.* **2013**, *285*, 317–323. [[CrossRef](#)]
17. Akatsu, T.; Yamada, Y.; Hoshikawa, Y.; Onoki, T.; Shinoda, Y.; Wakai, F. Multifunctional porous titanium oxide coating with apatite forming ability and photocatalytic activity on a titanium substrate formed by plasma electrolytic oxidation. *Mater. Sci. Eng. C* **2013**, *33*, 4871–4875. [[CrossRef](#)] [[PubMed](#)]
18. Shozui, T.; Tsuru, K.; Hayakawa, S.; Osaka, A. Enhancement of in vitro apatite-forming ability of thermally oxidized titanium surfaces by ultraviolet irradiation. *J. Ceram. Soc. Jpn.* **2007**, *116*, 530–535. [[CrossRef](#)]
19. Uetsuki, K.; Kaneda, H.; Shirotsaki, Y.; Hayakawa, S.; Osaka, A. Effects of UV-irradiation on in vitro apatite-forming ability of TiO₂ layers. *Mater. Sci. Eng. B* **2010**, *173*, 213–215. [[CrossRef](#)]
20. Uetsuki, K.; Nakai, S.; Shirotsaki, Y.; Hayakawa, S.; Osaka, A. Nucleation and growth of apatite on an anatase layer irradiated with UV light under different environmental conditions. *J. Biomed. Mater. Res. Part A* **2013**, *3*, 712–719. [[CrossRef](#)]

21. Lee, T.C.; Koshy, P.; Abdullah, H.Z.; Idris, M.I. Precipitation of bone-like apatite on anodised titanium in simulated body fluid under UV irradiation. *Surf. Coat. Technol.* **2016**, *301*, 20–28. [CrossRef]
22. Lee, T.C.; Abdullah, H.Z.; Koshy, P.; Idris, M.I. Ultraviolet-assisted biomimetic coating of bone-like apatite on anodized titanium for biomedical applications. *Thin Solid Films* **2018**, *660*, 191–198. [CrossRef]
23. Hanaor, D.A.; Sorrell, C.C. Review of the anatase to rutile phase transformation. *J. Mater. Sci.* **2011**, *46*, 855–874. [CrossRef]
24. Penn, R.L.; Banfield, J.F. Formation of rutile nuclei at anatase {112} twin interfaces and the phase transformation mechanism in nanocrystalline titania. *Am. Mineral.* **1999**, *84*, 871–876. [CrossRef]
25. Ricci, P.C.; Carbonaro, C.M.; Stagi, L.; Salis, M.; Casu, A.; Enzo, S.; Delogu, F. Anatase-to-rutile phase transition in TiO₂ nanoparticles irradiated by visible light. *J. Phys. Chem. C* **2013**, *117*, 7850–7857. [CrossRef]
26. Anatase, Wikipedia, the Free Encyclopedia. Available online: <https://en.wikipedia.org/wiki/Anatase> (accessed on 25 December 2018).
27. NIST (National Institute of Standards and Technology) XPS Database Selected Element Search Menu. Available online: <http://srdata.nist.gov/xps/selEnergyType.aspx>. (accessed on 20 November 2018).
28. Yang, G.Q.; Li, Z.H.; Lin, Z.X.; Wang, X.X.; Liu, P.; Fu, X.Z. Investigation of TiO₂ photocatalytic degradation of bovine serum albumin. *Guang pu xue yu guang pu fen xi= Guang pu* **2005**, *25*, 1309–1311. [PubMed]
29. Bouhekka, A.; Bürgi, T. Photodegradation of adsorbed bovine serum albumin on TiO₂ anatase investigated by in-situ ATR-IR spectroscopy. *Acta Chim. Slov.* **2012**, *59*, 841–847.
30. Yamamoto, H.; Demura, T.; Morita, M.; Kono, S.; Sekine, K.; Shinada, T.; Nakamura, S.; Tanii, T. In situ modification of cell-culture scaffolds by photocatalytic decomposition of organosilane monolayers. *Biofabrication* **2014**, *6*, 035021. [CrossRef]
31. Meusel, H.; Elshorbany, Y.; Kuhn, U.; Bartels-Rausch, T.; Reinmuth-Selzle, K.; Kampf, C.J.; Li, G.; Wang, X.; Lelieveld, J.; Poschl, U.; et al. Light-induced protein nitration and degradation with HONO emission. *Atmos. Chem. Phys.* **2017**, *17*, 11819–11833. [CrossRef]
32. Tu, M.; Abbood, H.A.; Zhu, Z.N.; Li, H.L.; Gao, Z.H. Investigation of the photocatalytic effect of zinc oxide nanoparticles in the presence of nitrite. *J. Hazard. Mater.* **2013**, *244*, 311–321. [CrossRef]
33. Tu, M.; Huang, Y.; Li, H.-L.; Gao, Z.-H. The stress caused by nitrite with titanium dioxide nanoparticles under UVA irradiation in human keratinocyte cell. *Toxicology* **2012**, *299*, 60–68. [CrossRef] [PubMed]
34. Greenwood, D.J.; Lees, H. Studies on the decomposition of amino acids in soils. *Plant Soil* **1960**, *12*, 69–80. [CrossRef]
35. Weiss, I.M.; Muth, C.; Drumm, R.; Kirchner, H. Thermal decomposition of the amino acids glycine, cysteine, aspartic acid, asparagine, glutamic acid, glutamine, arginine and histidine. *BMC Biophys.* **2018**, *11*, 2. [CrossRef] [PubMed]

